RANS SIMULATION OF TURBULENT SWEPT FLOW OVER A WIRE IN A CHANNEL FOR CORE THERMAL HYDRAULIC DESIGN USING K-EPSILON TURBULENCE MODELS

Byung-Hyun You, Yong Hoon Jeong*
Department of Nuclear and Quantum Engineering
Korea Advanced Institute of Science and Technology
291, Daehak-ro, Yuseong-gu, Daejeon, 305-701, Republic of Korea
bhyou@kaist.ac.kr; jeongyh@kaist.ac.kr

Yacine Addad
Department of Nuclear Engineering
Khalifa University of Science, Technology & Research
P.O.Box 127788, Abu Dhabi, UAE
yacine.addad@kustar.ac.ae

ABSTRACT

This paper presents a thermal hydraulic investigation of a nuclear reactor core, which is one of the most important components in the design of a nuclear power plant. Helical wire-wrapped fuel assemblies have been suggested for coolant mixing, and from a design point of view, an understanding of the influence of the reattachment length and recirculation bubbles could aid in determining the structural parameters for an optimal core thermal hydraulic design. In this study, assessments of Reynolds Averaged Navier-Stokes (RANS) based turbulence models were performed under various flow conditions for a wire in a channel. The calculation results were compared with the DNS results in terms of mean flow analysis and turbulent kinetic energy for further thermal hydraulic design of a wire-wrapped fuel assembly reactor core. The k-epsilon models with a two-layer wall treatment were chosen to predict the turbulent statistics of flow for four cases of a Reynolds equivalent flow rate of 0 to 1,709 along the cross-flow direction and an identical axial flow rate of 5,400. The selected standard k-epsilon models with three different constitutive relationships and a realizable k-epsilon model with the two-layer approach as the turbulence model revealed the locations of flow characteristics of interest, especially recirculation and reattachment, and showed that axial and cross-flow directional velocity profiles are fairly well matched. Relative to the DNS results, the errors in terms of reattachment lengths are approximately 1% for proper turbulence models in each case. From the well-matched flow modeling results and economical computing resources of the k-epsilon model, we conclude that this approach offers sufficient capability as an engineering design tool for core thermal hydraulics.

KEYWORDS
RANS simulation, k-epsilon, wire-wrapped fuel pin, core thermal hydraulic design

1. INTRODUCTION

This study focuses on the thermal hydraulic investigation of a nuclear reactor core, which is one of the most important components in the design of a nuclear power plant. Helical wire-wrapped fuel assemblies have been suggested for coolant mixing, and the helical wire structure generates a swept flow over a wire in the

sub-channels that can affect the temperature and mass flux distribution due to complex flow behaviors. This approach has been examined in a series of research studies on sub-channel analysis of a wire-wrapped fuel assembly using commercial computational fluid dynamics (CFD) codes based on the Reynolds average Navier-Stokes (RANS) turbulent models. Gajapathy et al. [1] performed thermal hydraulic analysis on a 7-pin wire-wrapped fuel bundle assembly using the k-epsilon turbulence model and investigated the velocity distributions in the axial and transverse directions and the temperature distribution with the suggested turbulence friction factor. An extendibility study of the 217-pin fuel bundle from the 7-, 19- and 37-fuel pin bundles was also performed by Gajapathy et al [2]; this research compared the friction factor for various Reynolds numbers against an experimental correlation reported by Novendetern, [3]. More recent publications [4-6] concentrated on a quantitative CFD benchmark in terms of velocity, temperature and pressure distribution; the CFD results were collected at Oak Ridge National Laboratory in the 1970s [7].

Ranjan et al. [8] performed direct numerical simulation (DNS) of turbulent swept flow in a stream-wise de-correlated rectangular channel with a wire-wrapped rod bundle as the obstacle structure. This group investigated the turbulent statistics of three-dimensional flow behaviors in a wire-wrapped channel along the axial and perpendicular directions of the wire. The particular locations of the reattachment point and the center of the recirculation bubbles were strongly related to the shear stress layer in four steps of changes in the Reynolds number equivalent flows across the wire. Pin-wire modeling studies were done in the exact same geometry with Ranjan's case by Merzari et al. [9]. They mainly performed large eddy simulation (LES) and RANS for predicting hot spot at different contact angles and gap sizes. The purpose of the current study is assessment of RANS-based turbulence model prediction in turbulent swept flow as a design tool for wire-wrapped fuel assemblies via validation with the DNS results. Standard k-epsilon models with linear and non-linear constitutive relationships and realizable k-epsilon models were chosen as a turbulent model with a two-layer wall treatment approach for observation of the flow behavior. We focus on the fluid characteristics along the shear stress layer and the turbulence kinetic energy distributions for selected turbulence models.

2. FLOW DESCRIPTION

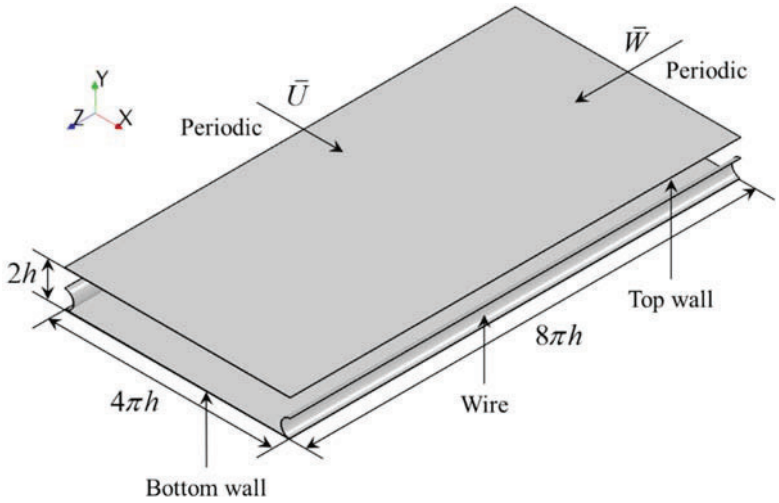

Figure 1. Schematic of the geometry modeled in the present study.

A rectangular channel with a circular obstacle was provided to matches that of the reference DNS calculation. As shown in the Figure 1, the size of the fluid domain is $4\pi h \times 2h \times 8\pi h$ based on the height of obstacle h along the x-, y- and z-directions, respectively. Each x-, y- and z-axis denotes the cross-flow

direction, vertical direction and the axial direction, respectively. Two pairs of inlet and outlet boundary conditions along the cross-flow direction and stream-wise direction are considered as the periodic boundary, and the other structures are modeled as a no-slip wall boundary of the flow channel. For geometrical modeling of contact between the channel and wire, restrictions exist due to the 180° contact angle tangencies. We chose to impose a radial displacement of the circular wire structure in the rectangular flow channel for approximately 2 % of the wire diameter to avoid numerical errors in the critical line contact region. Pressure gradients of each periodic boundary condition, which result from the adopted constant flow rates in four cases, drive the certain flow and bubble behavior in the channel. In this study, the flow rate of each direction is selected from the reference DNS simulation parameters for a single flow rate in the axial direction with four different and relatively lower flow rates in the cross-flow direction. Large recirculation bubbles formed in the leeward side of the wire following the shear stress layer that began at the top of the wire and ended at selected locations of the bottom wall.

3. SIMULATION PARAMETERS

3.1. Boundary Conditions

The flow is defined by the characteristic velocity and the length scale of each periodic inlet boundary. These characteristic scales are defined by the equivalent Reynolds numbers along the axial direction and cross-flow direction. The flow rates are defined in a general formula based on the channel surface area and the average cross-flow and axial flow velocity components U and W, respectively.

$$Q_z = \iint_S W(x,y)\,dxdy \tag{1}$$

$$Q_x = L_z \int U(x,y)dy \tag{2}$$

In the present study, the flow is characterized by the bulk axial velocity W_b and the height of the obstacle structure h. Based on these two characteristics of velocity and length scale, the Reynolds number in the axial and cross-flow direction is defined by equation (3) and (4) for each corresponding direction of the bulk velocity, respectively.

$$Re_z = \frac{\rho W_b h}{\mu} \tag{3}$$

$$Re_x = \frac{\rho U_b h}{\mu} \tag{4}$$

$$W_b = Q_z / S \tag{5}$$

$$U_b = Q_x / \left(2hL_z\right) \tag{6}$$

The bulk Reynolds number is defined as follows.

$$Re_b = \sqrt{Re_x^{\,2} + Re_z^{\,2}} \tag{7}$$

In the present study, all cases are adopted from the reference DNS calculation. With an identical axial flow rate equivalent to a 5,400 Reynolds number, four simulations labeled as cases A, B, C and D were defined by varying the flow rates along the cross-flow direction. The equivalent Reynolds numbers of the flow rates for each base are listed in Table I. In cases A through D, the cross-flow rate is increased to investigate the turbulent statistics of the flow bubble behavior in different situations. Using the characteristic parameters and the formulas, an inverse operation was applied to generate the input of the periodic boundary conditions.

Both the cross-flow and axial directional periodic boundary conditions are considered fully developed with a constant mass flow rate and the resulting pressure jump. The translational periodic interfaces were generated in each direction, and 100% of conformal matching was satisfied for the opposite side (and vice versa).

Table I. Simulation parameters for all cases

Case	Re_z	Re_x	Re_b	Q_z	Q_x
A	5,400	0	5,400	21.94	0
B	5,400	417	5,416	21.94	3.49
C	5,400	842	5,465	21.94	7.05
D	5,400	1,709	5,664	21.94	14.32

3.2. Turbulence Models

Two-equation turbulence models are based on the two important terms related to the turbulent kinetic energy and dissipation rate k and ε, respectively. We selected standard k-epsilon models with linear and non-linear constitutive relationships to observe the anisotropic effect on the flow. The standard k-epsilon model with a linear constitutive relationship stemmed from the Boussinesq approximation, which stated that the Reynolds stresses might be proportional to the mean rates of deformation. In this relationship, the viscous stress tensor depends on the turbulence, which adjusts itself as it is convected through the flow domain only. To allow for the anisotropic turbulence effect, quadratic and cubic non-linear constitutive relationships were suggested by extension of the Boussinesq approximation. In the quadratic relationship, the rate of change of the mean strain rate is treated as a partial account of the Reynolds stress transport. Furthermore, Craft et al. [10] suggested a cubic relationship by including cubic functions of the velocity gradient together with the quadratic relationship for improved sensitivity. These non-linear constitutive relationships offer the potential to capture anisotropy effects in the standard k-epsilon model.

The standard k-epsilon model is well known in modeling of turbulent flow in computational fluid dynamic fields; however, it encounters limitations for flows with a high mean shear rate or a massive separation due to over-predicted eddy viscosity. To improve the capability of the k-epsilon model, Shih et al., [11] suggested a new formulation for the dissipation rate equation and the eddy viscosity in terms of a realizable k-epsilon turbulent model based on the standard k-epsilon model with a realizable eddy viscosity model. In the standard k-epsilon model, the turbulent viscosity is computed from the constant C_μ. However, in the realizable k-epsilon model, the coefficient C_μ is no longer a constant but is imposed with the strain rate tensor and the vorticity tensor. All related constants have default values in the user manual of STAR-CCM+ v.9.02.011 [12].

3.3. Computational Grid

For proper turbulence modeling, the law of the wall must be satisfied to describe the flow behavior near the wall surface. To estimate the desired y^+ for applying the turbulence model, the related variables are calculated from the Reynolds number in the boundary layer in each case. For a turbulent boundary layer over a flat plate, the 99% boundary layer thickness is calculated from the bulk Reynolds number and the channel characteristic length. To adopt the boundary layer thickness, we estimated the Reynolds number in the 99% boundary layer and the skin friction coefficient using the Schlichting skin-friction correlation. Finally, the friction velocity was calculated to generate computational grids that agree with the viscous sub-layer wall treatment model.

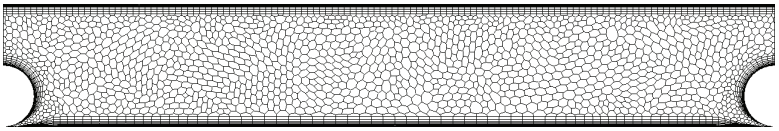

Figure 2. Computational mesh nodes in the *x-y* plane.

In STAR-CCM+, unstructured mesh generation is imposed with various base cell shapes. In the present study, polyhedral mesh and prism layer adaptation was selected as the mesh generation model. For the periodic boundary calculation, both the inlet and outlet side cells were perfectly matched in terms of shape and number of nodes. Near the wall boundary, 10 prism layers were stacked for satisfactory resolution in the viscous sub-layer. Overall, y^+ is less than 1 for the two-layer wall treatment approach. Mesh refinement were performed until reaching the specified accuracy for convergence. In Figure 2, the generated computational mesh alignment is represented on the *x-y* plane and shows that the above requirement is satisfied.

4. RESULTS

Information on the flow behavior and velocity profiles is provided in this section. Along the cross-flow direction, the particular locations of the reattachment and the center of the recirculation bubble were investigated via projection of streamlines on the *x-y* plane. The percent error is defined as the difference between the RANS simulation results and the DNS results.

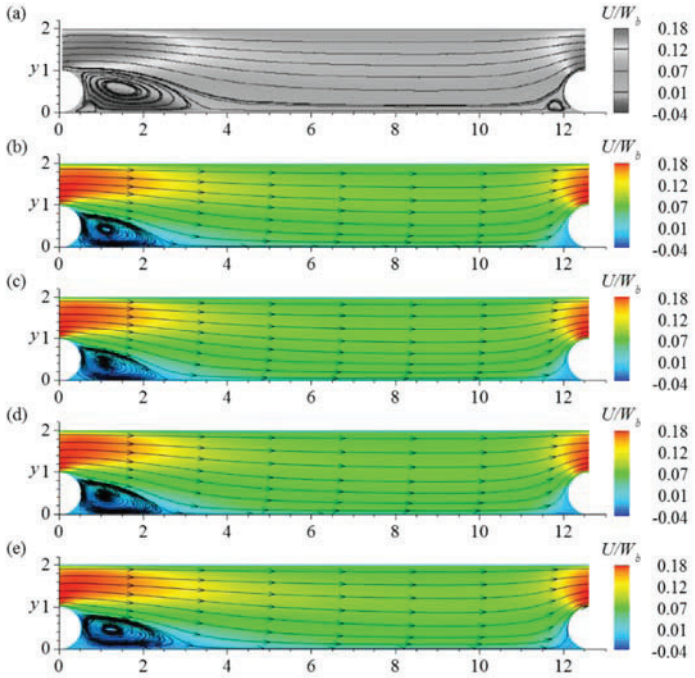

Figure 3. Iso-contours of the mean cross-flow velocity normalized by W_b and two-dimensional projection of the mean streamlines of (a) DNS, (b) standard k-epsilon with linear constitutive relationship, standard k-epsilon with non-linear (c) quadratic, (d) cubic relationship and (e) realizable k-epsilon for case B.

Figures 3 to 5 show the tangential streamlines and normalized cross-flow velocity gradients on the *x*-*y* plane in the flow channel. The tendency of the structure of the recirculation bubble formed by the cross-flow is similar to that of the DNS results. Recirculation bubbles are formed near the leeward side of the wire starting from the top of the wire to a particular location along the cross-flow direction. One major difference from the DNS results is the size of the secondary bubbles between the recirculation bubbles and the leeward side of the wire. In all cases of cross-flow, barely formed secondary bubbles are observed that are similar in size to the bubbles at the opposite side of the wire, which affects the formation of the primary bubbles in terms of the center location of the recirculation zone. The reattachment location is defined as the cross-flow location where the shear stress changes sign, i.e., in the same manner as the DNS reference. For clear comparison with the DNS results, we estimated the particular locations of the points that determine the structure of recirculation bubbles.

The maximum velocities are observed at the top of the wire region for all cross-flow cases due to the acceleration from the leeward side. In the bottom of the recirculation zone, which has a negative or opposite direction, the maximum velocities are shown by the backflows. Figures 6 to 8 represents velocity profiles in selected locations which are denoted by x_c, x_t, x_b and x_r, correspond to the center of the channel, top of the wire structure, the center of the recirculation bubbles and the reattachment point, respectively.

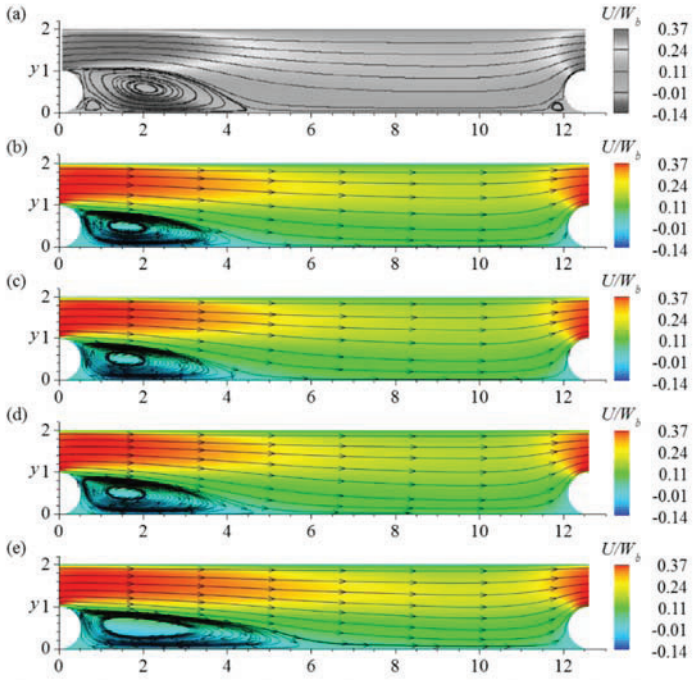

Figure 4. Iso-contours of the mean cross-flow velocity normalized by W_b and two-dimensional projection of the mean streamlines of (a) DNS, (b) standard k-epsilon with linear constitutive relationship, standard k-epsilon with the non-linear (c) quadratic, and (d) cubic relationship and (e) realizable k-epsilon for case C.

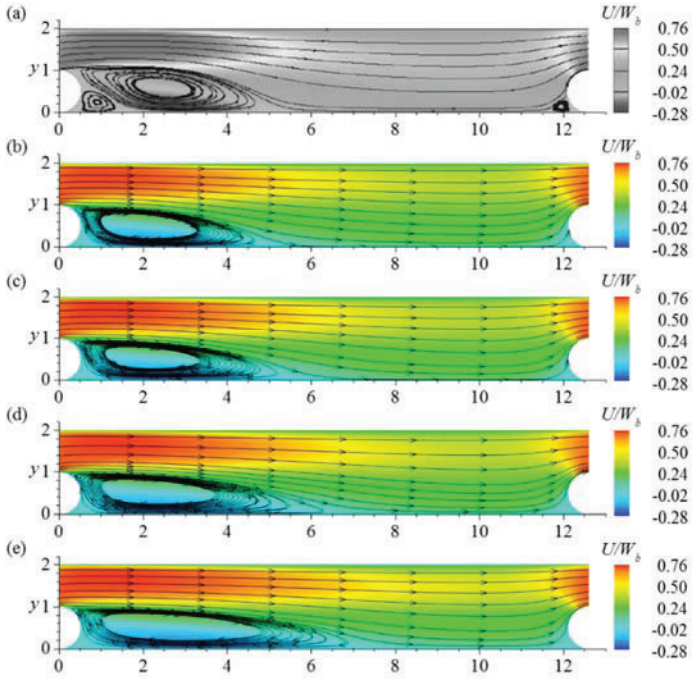

Figure 5. Iso-contours of the mean cross-flow velocity normalized by W_b and two-dimensional projection of the mean streamlines of (a) DNS, (b) standard k-epsilon with linear constitutive relationship, standard k-epsilon with the non-linear (c) quadratic, (d) cubic relationship and (e) realizable k-epsilon for case D.

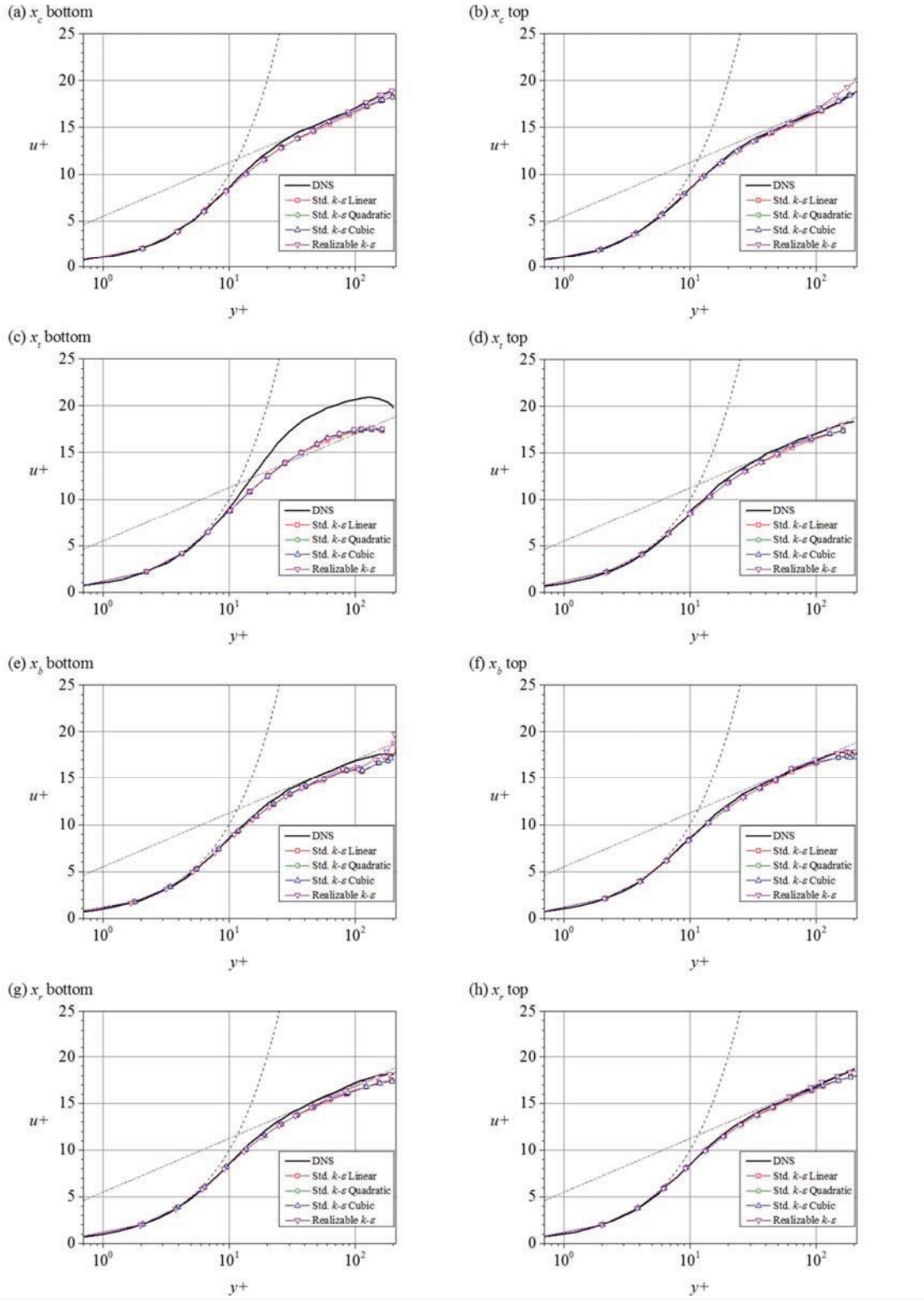

Figure 6. Profiles of mean velocity normalized by the friction velocity at different cross locations for case B.

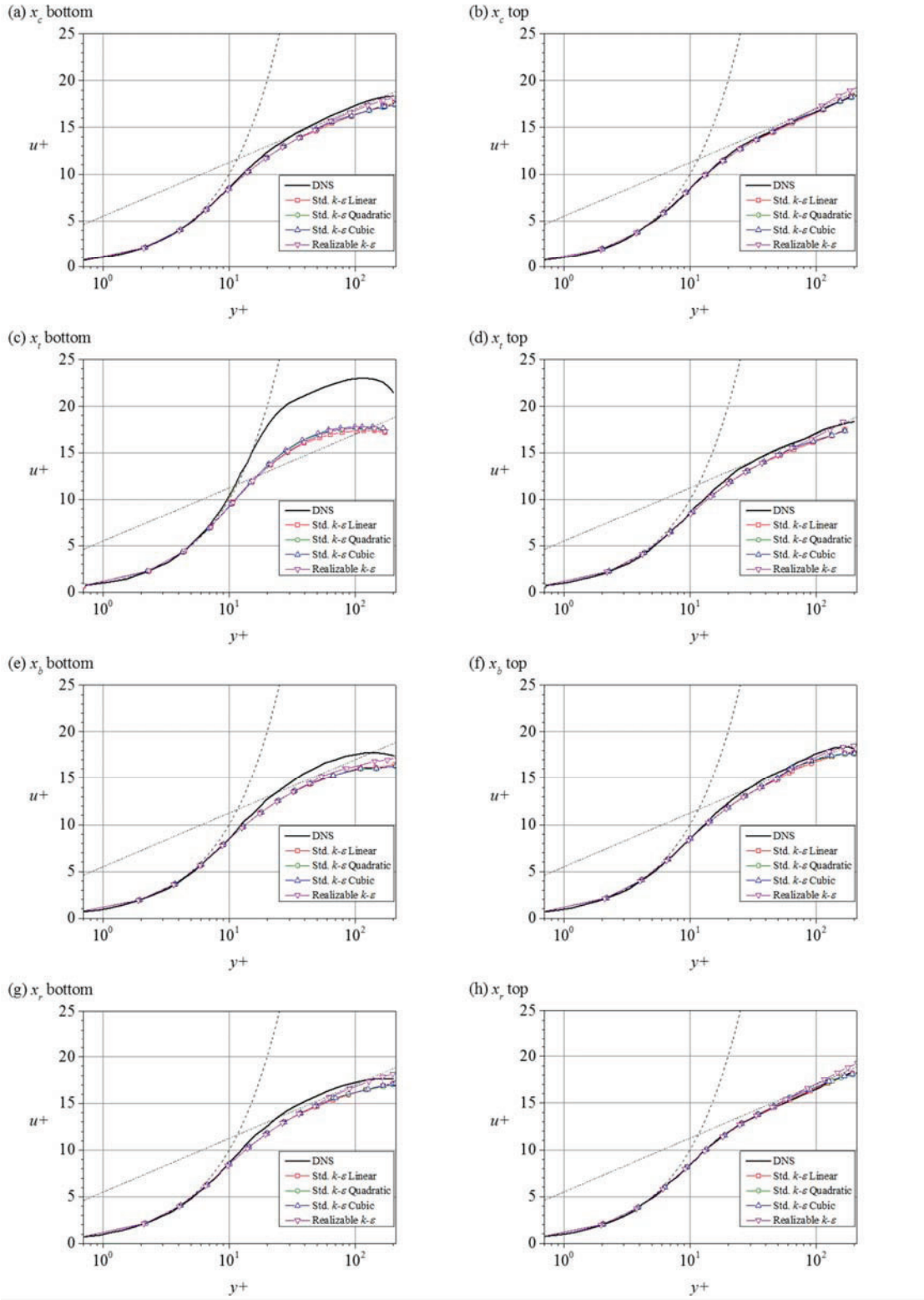

Figure 7. Profiles of mean velocity normalized by the friction velocity at different cross locations for case C.

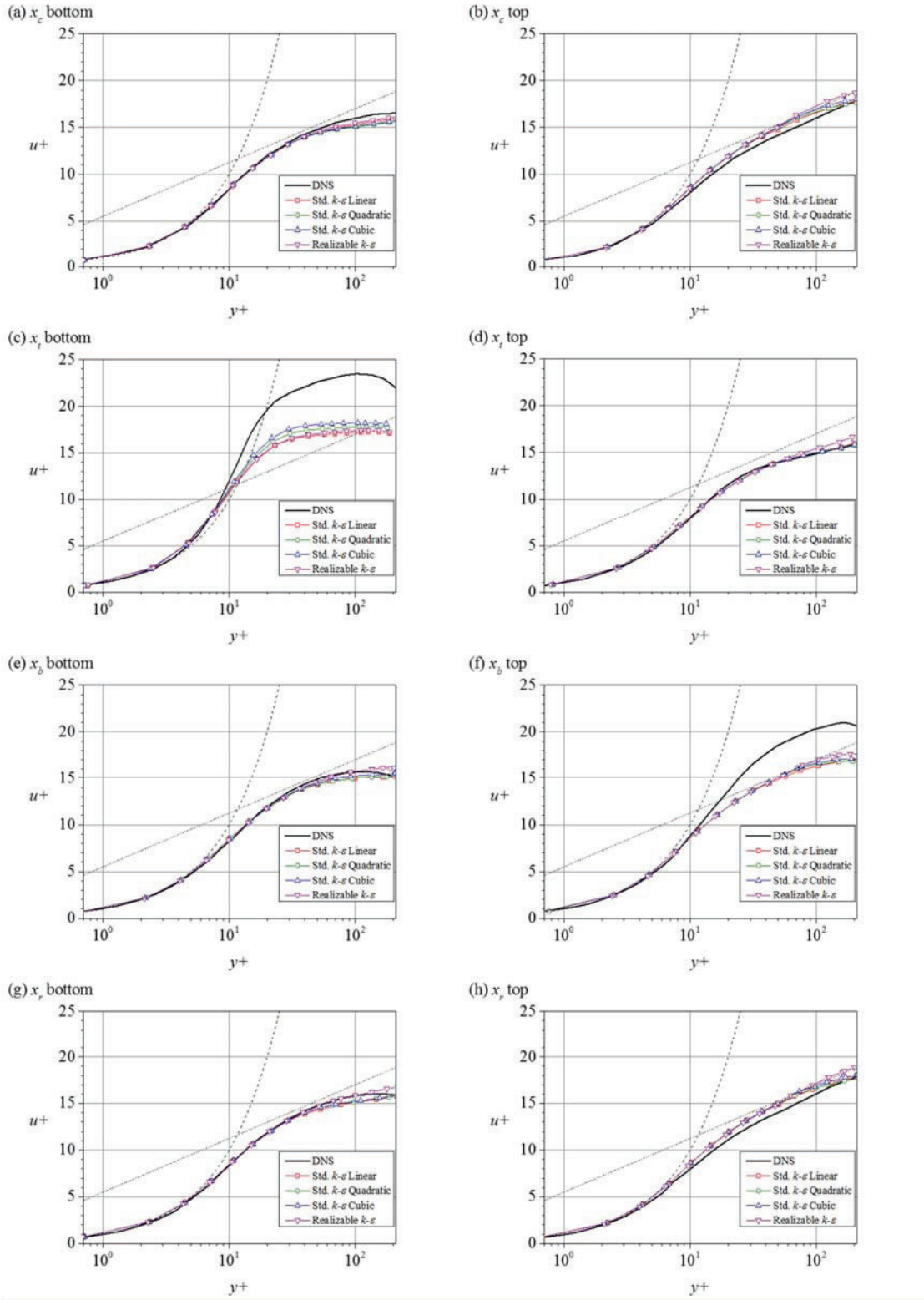

Figure 8. Profiles of mean velocity normalized by the friction velocity at different cross locations for case D.

Table II. Particular locations of the primary recirculation bubble structure and displacement errors along the cross-flow direction

	Case B			
	x_b	x_r	Error (x_b)	Error (x_r)
DNS	1.39	3.32	-	-
Std. k-ε Linear	1.15	2.71	1.91 %	4.85 %
Std. k-ε Quadratic	1.15	2.71	1.91 %	4.85 %
Std. k-ε Cubic	1.15	2.71	1.91 %	4.85 %
Realizable k-ε	1.25	3.21	1.11 %	0.88 %
	Case C			
	x_b	x_r	Error (x_b)	Error (x_r)
DNS	2.01	4.67	-	-
Std. k-ε Linear	1.67	4.75	2.71 %	0.64 %
Std. k-ε Quadratic	1.67	4.75	2.71 %	0.64 %
Std. k-ε Cubic	1.68	4.92	2.63 %	1.99 %
Realizable k-ε	1.98	6.08	0.24 %	11.22 %
	Case D			
	x_b	x_r	Error (x_b)	Error (x_r)
DNS	2.46	5.55	-	-
Std. k-ε Linear	2.01	5.80	3.58 %	1.99 %
Std. k-ε Quadratic	2.11	6.64	2.79 %	8.67 %
Std. k-ε Cubic	2.15	7.27	2.47 %	13.69 %
Realizable k-ε	2.52	8.15	0.48 %	20.69 %

Table II represents the particular locations of the recirculation bubble structure and displacements resulting from use of different k-epsilon models compared with the DNS results. For the minimum cross-flow rate of case B, the reattachment location is well matched using a realizable k-epsilon model with 0.88% displacement error. All of the standard k-epsilon models with different constitutive relationships give similar results. In case C, both the linear standard k-epsilon model and the non-linear quadratic standard k-epsilon model satisfactorily predict the recirculation behavior. The errors increase as more complex models are used compared with linear standard k-epsilon model. The maximum cross-flow case is fairly well predicted using the standard k-epsilon model, but the tendency of bubble dispersion is increased using other models.

5. CONCLUSION

Mean flow analysis was discussed, as normalized by the characteristic velocity W_b along the axial and cross-flow directions. As the cross-flow rate increases from case B to D, the shapes of the axial velocity gradient approach the leeward side of the wire structure. Each turbulence model gives different results in terms of recirculation bubble structures due to the different sensitivities of the anisotropic effect. In cases B, C and D, the minimum errors are observed using a standard k-epsilon model with linear constitutive relationships a realizable k-epsilon model. All errors are within 5% with use of proper turbulence models for individual cases with different ratios of cross-flow rate to axial flow-rate.

From an engineering design point of view, the RANS simulation is used to assess the prediction of turbulent statistics due to much lower resource requirements and shorter computation time. In the present study, the RANS simulation produced reasonable agreements with the DNS results in terms of mean flow distributions and the recirculation bubble structure. However, the proposed method must be treated carefully as the ratio

of the cross-flow rate to the axial flow rate is increased, e.g., a relatively lower mass flow rate than the normal operation condition at the inlet of the fuel assembly. In conclusion, the realizable k-epsilon model with a two-layer wall treatment model has sufficient capability to be used in further development of this tool for core thermal hydraulic design with a wire-wrapped fuel assembly.

ACKNOWLEDGMENTS

The authors gratefully acknowledge research support from the National Research Foundation of Korea (NFR) (Grant NRF-2013M2A8A6035681).

REFERENCES

1. R. Gajapathy, K. Velusamy, P. Selvaraj, P. Chellapandi and S. C. Chetal, "CFD investigation of helical wire-wrapped 7-pin fuel bundle and the challenges in modeling full scale 217 pin bundle," *J. Nucl. Eng. Des.* **237**, pp. 2332-2342 (2007).
2. R. Gajapathy, K. Velusamy, P. Selvaraj, P. Chellapandi and S. C. Chetal, "A comparative CFD investigation of helical wire-wrapped 7, 19 and 37 fuel pin bundles and its extendibility to 217 pin bundle," *J. Nucl. Eng. Des.* **239**, pp. 2279-2292 (2009).
3. E. H. Novendstern, "Turbulent flow pressure drop model for fuel rod assemblies utilizing a helical wire-wrap spacer system," *J. Nucl. Eng. Des.* **22**, pp. 19-27 (1972).
4. K. Natesan, T. Sundararajan, Narasimhan, Arunn and K. Velusamy, "Turbulent flow simulation in a wire-wrap rod bundle of an LMFBR," *J. Nucl. Eng. Des.* **240**, pp. 1063-1072 (2010).
5. Hamman, D. Kurt, Berry and A. Ray, "A CFD simulation process for fast reactor fuel assemblies," *J. Nucl. Eng. Des.* **240**, pp. 2304-2312 (2010).
6. J. W. Fricano and E. Baglietto, "A quantitative CFD benchmark for sodium fast reactor fuel assembly modeling," *Ann. Nucl. Energy.* **64**, pp. 32-42 (2014).
7. M. H. Fontana, R. E. MacPherson, P. A. Gnadt, L. F. Parsly, and J. L. Wantland, *Temperature distribution in a 19-rod simulated LMFBR fuel assembly in a hexagonal duct (Fuel failure mockup bundle 2A) – record of Experimental Data. Oak Ridge National Laboratory*, Oak Ridge National Laboratory, ORNL-TM-4113 (1973).
8. R. Ranjan, C. Pantano and P. Fischer, "Direct simulation of turbulent swept flow over a wire in a channel," *J. Fluid Mech.* **651**, pp. 165-209 (2010).
9. E. Merzari, W. D. Pointer, J. G. Smith, A. Tentner and P. Fischer, "Numerical simulation of the flow in wire-wrapped pin bundles: Effect of pin-wire contact modeling," *J. Nucl. Eng. Des.* **253**, pp. 374-386 (2012).
10. T. J. Craft, B. E. Launder and K. Suga, "Development and application of a cubic eddy-viscosity model of turbulence," *Int. J. Heat Fluid Fl.* **17**(2), pp. 108-115 (1996).
11. T. -H. Shih, W. W. Liou, A. Shabbir, Z. Yang, and J. Zhu, "A new k-e eddy viscosity model for high Reynolds number turbulent flows – model development and validation," *Computer Fluids.* **24**(3), pp. 227-238 (1994).
12. CD-adapco, 2014. STAR-CCM+ User Guide, Version 9.02.011. CD-adapco, New York.